applied sciences

MDPI

Article

Twenty Years of Progress in Microstructure Modelling for Ultrasonic Testing, from Shielded Metal Arc Welding to Gas Tungsten Arc Welding: An Analysis for Future Developments

Joseph Moysan *, Cécile Gueudré, Marie-Aude Ploix and Gilles Corneloup

Aix Marseille University, CNRS, Centrale Marseille, LMA UMR 7031, 13453 Marseille, France
* Correspondence: joseph.moysan@univ-amu.fr

Featured Application: Development of a precise Ultrasonic Testing of Welds using material modelisation : a solution and its development.

Abstract: To ensure and to demonstrate the mechanical integrity of a welded structure, precise ultrasonic testing (UT) is often mandatory. The importance of the link between nondestructive testing (NDT) and the assessment of structural integrity is recalled. However, it is difficult to achieve great efficiency as the welding of thick and heavy structural part produces heterogeneous material. Heterogeneity results from the welding process itself as well as from the material solidification laws. For thick components, several welding passes are deposited, and temperature gradients create material grain elongation and/or size variations. In many cases, the welded material is also anisotropic, this anisotropy being due to the metal used, for example, austenitic stainless steel. At the early stages of ultrasonic testing, this kind of welded material was considered too unpredictable, and thus too difficult to be tested by ultrasounds without possible diagnosis errors and misunderstandings. At the end of the 1990s, an algorithmic solution to predict the material organisation began to be developed using data included in the welding notebook. This algorithm or modelling solution was called MINA. This present work recalls, in a synthetic form, the path followed to create this algorithm combining the use of solidification laws and the knowledge of the order of passes in the case of shielded metal arc welding (SMAW). This work describes and questions the simplifications used to produce a robust algorithm able to give a digital description of the material for wave simulation code. Step by step, advances and demonstrations are described as well as the limitations, and ways to progress are sketched. Recent developments are then explained and discussed for modelling in the case of gas tungsten arc welding (GTAW), in addition to discussions about 3D modelling for the future. The discussion includes alternative ways to represent the welded material and challenges to continue to produce more and more convincing weld material model to qualify and to make use of UT methods.

Keywords: ultrasounds; ultrasonic testing; weld; multipass weld; modelling; stainless steel; nondestructive testing; anisotropic material; heterogeneous material

Citation: Moysan, J.; Gueudré, C.; Ploix M.-A.; Corneloup, G. Twenty Years of Progress in Microstructure Modelling for Ultrasonic Testing, from Shielded Metal Arc Welding to Gas Tungsten Arc Welding: An Analysis for Future Developments. *Appl. Sci.* **2023**, *13*, 10852. https://doi.org/10.3390/app131910852

Academic Editor: Giuseppe Lacidogna

Received: 31 July 2023
Revised: 18 September 2023
Accepted: 20 September 2023
Published: 29 September 2023

1. Introduction: Structural Integrity and Ultrasonic Testing

Ultrasonic testing (UT) is a standard method for carrying out nondestructive evaluation in large mechanical structures that need to be particularly monitored because of the extremely damaging consequences of their catastrophic failure. Asset integrity management has become a very important multidisciplinary and interprofessional activity in the aerospace, nuclear power generation, petrochemical, oil, fossil and gas production industries. Monitoring the mechanical integrity of structures relies heavily on nondestructive testing means to define the reality of defects resulting from the manufacturing process or from the life of the structure. More broadly, nondestructive methods are used to monitor the evolution of the mechanical properties of structures as well as the evolution of possible

damage. Steels still have a predominant role in large mechanical structures, and these structures are frequently connected by welding. Since the 1930s, welding has become an increasingly important part of the manufacturing process. The growing importance of this joining technique began with the Liberty Ships when welds replaced riveted joints, lightening the structure and allowing for smoother hulls [1]. However, they also have their drawbacks: residual stresses, manufacturing or fatigue defects such as cracks, inclusions and porosity. Nondestructive methods applied to weld inspection include a large number of well-known techniques, such as radiography, ultrasound, electromagnetic methods (eddy current, magnetic particle inspection) [2,3]. The choice of the best method for solving the problem posed (i.e., detection, characterisation or sizing) is the first essential step in any approach aiming at the nondestructive examination of a mechanical structure. For the inspection of welds, and particularly for the inspection of structures on site, ultrasonic inspection is often preferred because of its multiple possible implementations using surface waves, volume waves and guided waves of all types. Ultrasonic transducers generate high-frequency mechanical waves. Several kinds of propagating modes are possible, offering many solutions to component integrity investigation.

The development of probabilistic fracture mechanics has completely changed the role of NDT. Thanks to the combination of quantitative nondestructive evaluation with the probabilistic fracture mechanics approach, NDT has become a technology that can reduce costs and improve productivity. A particularly important development in France is the new regulations of 1999, concerning the safety of French nuclear power plants. In these new regulations, the maintenance objectives rely even more on the performance of nondestructive techniques [4,5]. For structures at the end of their lives, the question of the requalification of their structural integrity is also raised [6]. While there are well-developed codes or standards governing newly developed systems and equipment, there are still major gaps in the assessment of the mechanical and structural integrity of ageing facilities. Modelling requirements have become essential for quantifying measured quantities and for investigating the reliability of nondestructive methods. Integrity assessment includes the systematic identification of possible failures and the assessment of their probability and possible consequences. It also includes the development of strategies to avoid these failures, through the use of good practices in design, control operation and rehabilitation when necessary. Regular advances over many years in quantitative assessment have brought nondestructive methods to play an increasingly important role. They are integrated into global reliability assessment approaches [7–12]. Fault detection, characterisation and sizing are essential to this assessment process. Mainly, studies focus on cracks, which are the most dangerous defects because of their ability to propagate and because they are difficult to detect during inspections. Particular efforts to assess the behaviour of cracks submitted to thermo-mechanical loads have been made within the frame of the European programme SINTAP (Structural INtegrity Assessment Procedures) [11,13,14]. Probabilistic fracture mechanics provides a link between nondestructive measurements and mechanical integrity validation. For this type of calculation, it is very important to evaluate nondestructive reliability [15–17]. As fracture mechanics includes the idea of critical crack length for a given loading and nondestructive testing measures crack size, it is tempting to stop at this point. It is obvious that the link is not so simple, because of the simplifying assumptions (linearity, elasticity) of fracture mechanics and those of all nondestructive testing methods. For real cracks (rough and with complex shape), there is a need for experimental data to correlate their size from a fracture mechanics point of view with that obtained by nondestructive examination. Probabilistic fracture mechanics requires knowledge of the initial distribution of defects, to define crack growth laws [6,11,18,19]. Wu [18] proposes failure probabilities including probability of detection (POD) curves to demonstrate how in-service inspections improve the mechanical integrity of structures. Rouhan [6] defines a probability of local failure of a structure from the probabilities of detection and false alarms. Dillström [11] differentiates between crack detection and failure probability calculations. Singh [19] shows

the importance of knowing the capability of nondestructive means to realistically estimate the growth of damage in order to plan inspections that guarantee the safety of aircraft.

Predicting the reliability of detection from nondestructive measurements is, however, made complex by all the constraints outside the application of physical principles alone. Progress in nondestructive examination is limited by environmental constraints (in situ), design constraints (inaccessible areas) and material constraints (non-perfect), which are developed in this paper. Other difficulties are the use of codes and regulations limiting the development of new ideas and the difficulty to make technology transfer when it is multidisciplinary. The human factor is still very difficult to be taken into account in association with a scientific predictive approach such as POD. Both metrics are perhaps simply non-associative. Recent work has developed the analysis and modelling of human and organisational factors. In their work, Larouzee and al. developed the Cognitive Reliability and Error Analysis Method (CREAM) to achieve the interpretation of radiograms. Data were collected through a survey conducted with operators in a nuclear power plant [20]. In the case of the nuclear industry, it has been necessary to create reliable, large-scale benchmarks to study the reliability of NDT methods. The PISC (Programme for the Inspection of Steel Components) started in 1976 with the PISC I programme and was continued with PISC II (1980–1986) and PISC III (1988). These are major international programmes involving fifteen countries and some fifty NDT teams worldwide. Other trials of this type have also taken place on a smaller scale, such as the Defect Detection Trial (DDT, 1983), or in the aeronautical and offshore fields [21]. The need to create standard parts for NDT is still relevant today in every industrial field, as is the case for bonding in aeronautics [22,23]. These standard parts are essential to assess the efficiency of novelties in NDT techniques.

In general, ultrasonic methods have a fairly good average accuracy of defect sizing, but with a fairly high standard deviation [24]. This trend is confirmed in the PISC III tests where five out of seven teams overestimate the defects. The average sizing error in these tests is only 0.5 mm for a maximum crack size of 30% of the wall thickness. Such an average value may seem good, but this performance should be put into perspective, because the correlation between the size assessed by the nondestructive examination and the real size still shows a large dispersion [25]. In general, if the checks by different teams are multiplied, the risk of leaving an unacceptable defect undetected drops considerably. The best sizing results are obtained by using the crack tip diffraction echo, which encourages the use of focused sensors [26]. The poor fatigue crack detection performance is due to the material structure of the steels used. The best performances are obtained in ferritic forged steels with easy access. The performance decreases with accessibility difficulties and becomes even worse in welds sometimes at very low levels [25]. The best results are obtained in welds for automatic processes and for detection methods just above the noise level. Conversely, this configuration often leads to more false alarms [25,27,28]. With the beginning of numerical simulations for NDT applications, it was understandable that an alternative to standard blocks was to build simulators which took into account the many causes of amplitude variations and signal noise [15]. Year after year, numerous physical laws have been progressively included in specialised software, such as the CIVA code [29], and the POD (probability of detection) is now a part of research work in NDT science [30].

In the last twenty years, mechanical integrity assessment has been progressing, with a better understanding of the physical and mechanical phenomena underlying nondestructive characterisation. This has required bringing together many scientific skills. We are contributing to the understanding of ultrasonic testing in anisotropic and heterogeneous welds by developing welded material modelling as well as by developing experimental setups allowing for the validation of the latest developments in numerical modelling. Figure 1 in the next section illustrates this methodology we are building to improve UT reliability.

In this paper, we describe the progression of ideas for a phenomenological approach for describing the mechanical parameters of a welded material. The analysis of the advances in material modelling for ultrasonic testing of welds begins in Section 1 with the description of the initial requirements of material modelling for anisotropic and heterogeneous welds, as the

numerical modelling of ultrasonic testing requires wave propagation modelling. The material issue is presented with a literature survey. In Section 2, the phenomenological model, MINA, is explained. The MINA method relies on the study of solidification laws during the welding process. Taking into account information from the welding notebook, a set of grain growth rules was implemented in a model for shielded metal arc welding (SMAW). As gas tungsten arc welding (GTAW) has many advantages for industrial welding, there was a need to extend the MINA model to the GTAW process. The corresponding studies are developed in Section 3. As complete models are now available, an inverse approach is possible for improving the knowledge about the welded material. In Section 4, a discussion is held on inverse approaches for improving or defining grain orientation maps. In the conclusion, future possible developments are suggested from the latest studies in the field.

2. Material Modelling for Anisotropic and Heterogeneous Welds

2.1. The Material Issue

To understand the results of ultrasonic testing, it is of particular importance to know the grain orientation resulting from the material solidification during the welding process. Part 1 in Figure 1 shows a classical micrograph of a multipass weld produced using a metallography analysis. The grain orientation is heterogeneous, with possible strong change in the grain direction as underlined with the purple line in the zoomed part of Part 1. Because of the diameter of the ultrasonic beam, this causes beam deviation and division, as the front wave does propagate in a heterogeneous medium. The methodology is to understand physical mechanisms of grain growth to propose a grain orientation model to be able to propose a complete welded material modelling.

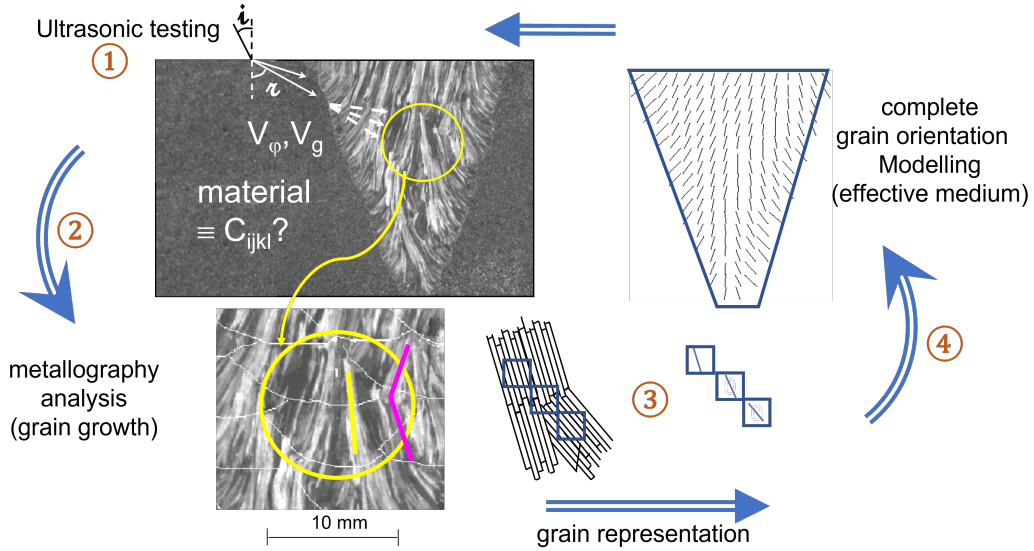

Figure 1. Methodology to describe material for UT in anisotropic and heterogeneous welds.

Using the formalism detailed in [31], Equation (1) is the elastic wave equation (or elastodynamic wave equation), showing that particle displacement u depends on the elasticity constants C_{ijkl}. This first equation leads to the known Christoffel equation (Equation (2)).

$$\rho \frac{\delta^2 u_i}{\delta t^2} = C_{ijkl} \frac{\delta^2 u_k}{\delta x_j \, \delta x_l} \tag{1}$$

$$\rho {V_\varphi}^2 \delta_{il} - C_{ijkl} n_j n_k = 0 \tag{2}$$

In these equations, ρ is the density and V_φ the phase velocity. The Kronecker symbol is δ_{il}. n_j and n_k are coordinates of n, the propagation direction. In the general case for an anisotropic material, three solutions are calculated for each wave direction. Three group

velocities (V_g) are related to the propagation of the energy, and the phase velocity V_φ is the wavefront velocity. The angle of deviation between these two velocities depends on the wave type, and may reach about 45° in the case of a vertical transverse wave. These results are schematised in Figure 1 Part 1: depending on the incident angle i and the Snell law, up to three elastic waves are refracted with various angles r in the material, and they are transmitted and reflected at any further material interfaces, such as grain interfaces. All the following waves' properties are calculated using the same equations, Equations (1) and (2). Elasticity constants C_{ijkl} are thus the first data to fix. An austenitic grain is usually considered an orthotropic material. The tensor values of the elastic constants (or stiffness tensor) found in the literature show significant variations depending on the steel composition. Measurements of such material properties are difficult. The grain direction can be obtained by X-diffractometry and elastic constants can be evaluated by ultrasound setups. An inverse method is used with the same equations to calculate wave velocities. Velocities are measured for various angles of incidence. Parallelepipedic samples have been cut in the weld to evaluate the elastic constants with good certainty [32,33]. These elastic constants correspond to the orthotropic properties related to the longitudinal orientation of a columnar grain. This principal orientation is assimilated to a <1 0 0> crystallographic direction. This direction corresponds to a local coordinate system. This hypothesis is validated with various crystallographic analyses by EBSD and by X-diffractometry. During the welding process, the metal solidification can create diverse grain structures, and thus very different grain orientations. The resulting material is anisotropic, but nearly as importantly, this welded material is heterogeneous. The wave front is transmitted through the same orthotropic material, but as the wave front is not aligned with the grain direction, the apparent elastic constants are modified along the wave propagation direction. The material description becomes as complex as that of a triclinic material. Beam deviation, beam distortion and even beam division are observed in multipass welds [33]. For thick components, epitaxial growth elongates grains, and combined with a reduced beam quality, the grain noise increases, thus decreasing the probability of detection. On the opposite side, due to beam deviation combined with particularly large grains, false detection occurs. All these phenomena were studied from the beginning of UT, but numerical simulation began really during the 80s when equations were implemented for the first time. As the grain orientation follows macroscopic temperature gradients in the weld, it is not randomly distributed. This is where grain modelling comes in.

2.2. First Grain Modelling for Wave Propagation Simulation

In the literature, authors proposed models of grain structures to describe materials for simulations. The description of grain structure is frequently simple. The proposed structure is mainly symmetrical for obvious practical reasons to reduce modelling complexity. But real structures are in general non-symmetrical. Figure 2 presents six examples of simulated grain structures, with the first interesting results for the analysis of UT results. In part (a), the grain structure proposed by Ogilvy [34] is represented and corresponding mathematical functions are given in Formula 3. Angles θ between grain direction and axis Oy are thus calculated and drawn in Figure 2 part (a) and part (b). The index i is equal to 1 or 2, allowing for a variation depending on the chamfer parameters, which could thus be non-symmetrical. Simulation of the wave propagation is obtained with the RAYTRAIM code, which calculates the wave central ray.

$$\tan\theta_i = \frac{T_i(D_i + z\tan(\alpha_i)}{y^\eta} \; for \; y > 0 \tag{3}$$

Therefore, this equation calculates the grain direction for the right part of the weld (i = 1) and the left part of the weld (i = 2). Several chamfer geometries can be defined, and also, the set of equations can be used to create a non-symmetrical grain structure. The parameter η range is comprised between 0 and 1. This parameter represents the orientation speed of the grains from the edge towards the vertical direction of the weld

vertical axis. Silk operates in the same way [35]. Spies also uses this type of structure by defining several layers of transverse isotropic material to describe the weld, as shown in part (c) of Figure 2 [36]. In his work, Schmitz uses the ray code 3D-Ray-SAFT to obtain the direction of ultrasound propagation with a 3D simulated grain structure. The grain orientation of an X-weld is expressed with a three-coordinate N orientation vector [37]. The grain structure starts perpendicular to the weld edges and ends vertically in the centre of the weld. Schmitz qualitatively compares the experimental CSCAN with the simulated CSCAN and observes a good agreement. Langenberg [38] also chooses a simplified symmetric weld grain structure ((part (d)) of Figure 2) to make use of the EFIT (Elastodynamic Finite Integration Technique) code. Quantitative comparisons are made between experimental and calculated images (BSCAN). Halkjaer [39] uses this code with the Ogilvy grain structure in transverse isotropic symmetry. If the grain structure develops into a non-symmetrical structure, Silk defines various homogeneous domains with different sizes (((part (e) and (f)) of Figure 2) [35]. Chassignole [33] uses the ULTSON 2D finite element code enabling the visualisation of the whole beam and not only of some rays. He introduces a complex grain structure in 2 × 2 mm^2 squares whose orientations correspond to those measured on a real multipass weld macrograph or proposes to model the structure using large areas by clustering in a bigger region several smaller regions of close orientations. The simulated BSCANs are comparable to the experimental BSCANs. The Champs-Sons semi-analytical code simulates the ultrasonic field for a homogeneous anisotropic material. Associated with the Mephisto code, which models the interaction of the beam with defects, it provides an efficient tool for modelling weld inspection [40,41]. This code has the advantage of being able to simulate ultrasound propagation in 3D geometries. In contrast to the ray methods, by integrating the brush method, this code makes it possible to describe the variation in the wave amplitude.

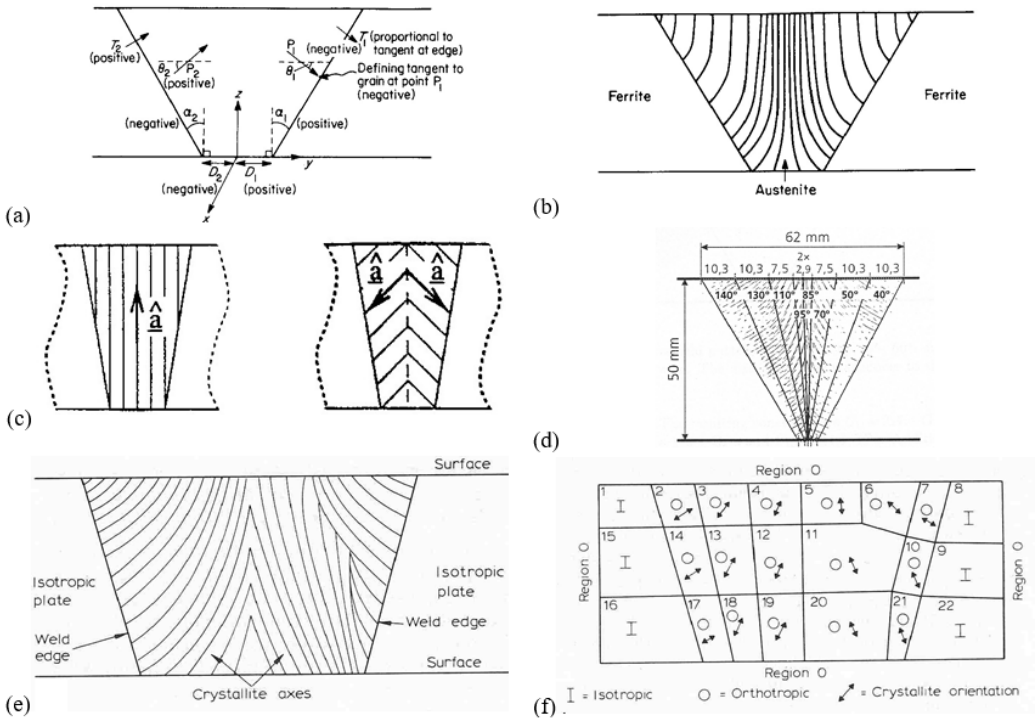

Figure 2. Compilation of several grain descriptions in heterogeneous welds in [42].

These ideas to describe an acoustically inhomogeneous anisotropic material continue to be tested regularly in various welding configurations in 2D situations, often using ray tracing models in 2D situations [43,44]. Material description is always the first step of a good UT simulation, even in the newest studies with modern tools, using, for example, phased array ultrasonic testing (PAUT) and a simulation code like CIVA [45].

In these previous studies, qualitative comparisons were made with experimental results, which proved rather good prediction quality, but improvement is needed for finer prediction. It should also be noticed that simulated welds do not represent the reality of a complex heterogeneous structure resulting from welding procedure. Furthermore, when multipass welds are realised, the grain structure is more complex. In the next section, we explain how a robust model was conceived by taking into account solidification laws.

3. Phenomenological Model: The MINA Model

3.1. The Importance of Solidification Laws during the Welding Process

Several grain structure prediction models have been developed that differ depending on the various welding processes available (electron beam, tungsten inert gas, coated electrode, laser, plasma, etc.). These models also differ depending on the material used such as steel, aluminium or titanium. There has been steady progress in welding modelling since the 1960s, when mainly the temperature gradient was taken into account. Substantial progress was made in the 1990s with studies on solidification mechanisms [46]. The goal was to define a correlation between the final microstructure and the solidification parameters [47]. In the case of austenitic steels, modelling is mainly performed using a two-dimensional approach. Models differ in the rules governing the initiation of crystal growth, in the progression of the grain boundary and in the change in the crystallographic orientation. What is difficult is the modelling of the links between the growth of the primary arms and the growth of the secondary arms of the dendrites [11,48]. The solidification of an austenitic stainless steel varies according to the Fe-Ni-Cr ternary alloy composition. The KGT model [49,50] assumes that dendrite formation is controlled by nickel diffusion, and assuming a constant weld pool, the model derives relationships between heat source displacement rates, solidification front velocity and dendrite tip growth rate. This model predicts the preferred solidification directions. Another important model is the CAFE model [51,52], which is a two-dimensional cellular automaton algorithm. It simulates dendritic grain formation. The model includes heterogeneous nucleation, growth kinetics and preferential growth directions. A finite element model based on an enthalpic method makes it possible to predict the growth of grains in the cells at each time step. The growth competition between grains is then simulated. In the literature, similar approaches have been developed for different welding processes [53–55]. It should be emphasised that the properties of the parent metal modify the texture of the welded joint, in particular the average grain size. Depending on the differences in composition and crystal structure between the base metal and the filler metal, epitaxial growth or heterogeneous nucleation can occur [56]. For thin sheets, the total melting of the welded thickness could be modelled. A flat solidification is observed, as well as the absence of secondary dendrite arms. The direction of grain growth is calculated by using the direction of the gradient and the directions of the two grains that meet during the solidification to decide on the resulting orientation. There are not yet models that deal with multipass welding, and work is being started in this area. Analytical models for predicting heat flux in this type of process are beginning to be proposed [57–59]. All these models are mainly concerned with automatic or semi-automatic processes and therefore do not take into account the particularities of the manual welding method.

3.2. The Use of the Welding Notebook and Grain Growth Rules

A phenomenological model was conceived from the analysis of multiple welds and by making tests with dedicated mock-ups. It is original in that it uses information contained in the welding notebook and does not develop a complete welding simulation. This model is called MINA, for Modelling anIsotropy from Notebook of Arc welding [60]. Variables, extracted from the notebook, used in this model are the number and the order of passes written down by the welder. Electrode diameters vary with the stacking of passes. This model as developed for shielded metal arc welding (SMAV) and uses metallography analysis of weld cross sections, and so is a two-dimensional model.

The thicknesses of passes (height h in Figure 3) are calculated using a proportional rule from electrode diameters, then pass widths (W) are calculated depending of their vertical position and the corresponding weld width. The algorithm has four parts: description of the temperature gradient directions in the weld pool, description of the remelting of passes, description of the incline of passes and calculation of the grain growth. The shape of the weld pool is defined from numerous metallography analyses. This geometry is described with two parabolic curves whose top points are O and C. The positions of points C and D are proportional to h [60]. From this weld pool simplified description, a formula is defined to calculate the direction of the local temperature gradient. The gradient direction comes from point D. The gradient angle measured from vertical is α_g. When a new pass fills the weld, laterally or vertically from the previous pass, this operation creates a partial remelting. Two parameters were introduced in the model: R_L, which is the lateral remelting rate; and R_V, which is the vertical remelting rate. They are the two most important variables to describe the grain structure in the MINA model.

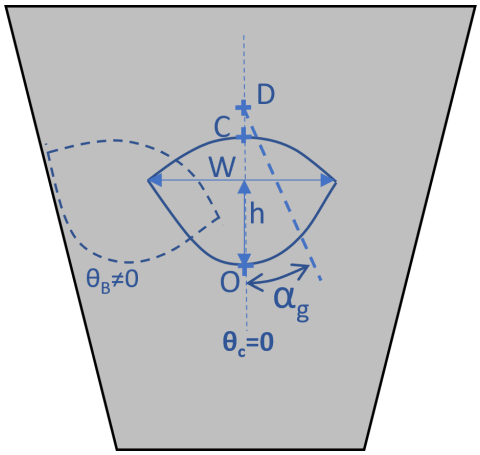

Figure 3. Simplified pass description in MINA model.

The analysis of the welder's gesture shows that the welder has to tilt his electrode during the pass deposit, causing a rotation of the welding pool. A simplified hypothesis for the MINA model is to consider that this phenomenon implies the rotation of the direction of the temperature gradient with no modification in the pass geometry. The analysis of the SMAW welding method combined with all our metallography observations leads us to separate two cases. If a pass is placed and leans on a previous pass, then the temperature gradient is considered to be inclined by an angle θ_C lower than the second angle, θ_B, which is observed if a pass leans on the sidewall. This angle θ_B represents in some way the impact of the weld geometry. When a pass fills the weld and leans both on its left and its right, the calculated temperature gradient is symmetric, so $\theta_C = 0$. The model MINA provides these two parameters θ_B and θ_C for each pass using the position of the pass written in the welding notebook.

The fourth part of the algorithm is the calculation of the grain growth. This growth is driven by three physical phenomena: epitaxial growth, influence of the temperature gradient, and selective growth. Selective growth results from the growth competition between grains. Epitaxial growth occurs when the fused metal in the new pass solidifies, keeping the crystalline orientation of the grain that is just below. Grains tend to follow preferentially the direction of the local temperature gradient, which can be considered to be perpendicular to the isotherms. Grain growth occurs at variable speeds. If a grain has its <1 0 0> crystallographic direction parallel to the heat flow direction, this grain grows rapidly, and so stifles the growth of unsuitably oriented ones. When their orientation is close to the heat flow direction, they turn towards this direction thanks to the growth of secondary arms. This phenomenon is the epitaxial: growth when grains make little turns to follow the direction of the gradient α_g. Taking into account these three main phenomena,

the algorithm calculates the resulting grain orientation, noted $\alpha(n)$. To reproduce the slow grain turn from its first direction towards the direction of α_g, and to reproduce the selective growth, the model uses an iterative formulation with also a scale factor. Formulae are applied n times in a mesh to simulate changes in grain orientation at a smaller scale. This model is supported by image analysis. Images come from metallographic etching on welds manufactured with the same welding notebook by two different welders [60]. For a typical scale of 2 × 2 mm^2, the value of n is fixed at 10.

The algorithm begins by the first pass at the bottom of the weld. For additional passes, the grain orientation is calculated in meshes with $\alpha(0)$, the grain orientation α_{inf} in a previous mesh. If a previous orientation is not close to the direction α_g, the new grain orientation, $\alpha(n)$, inclines strongly to this direction α_g. This represents the selective growth that eliminates badly oriented grains. If the angular difference is greater than 90°, it is considered that selective growth occurs directly, as described in formulae

$$n = 1, \alpha(0) = \alpha_{inf} \tag{4}$$

$$if(\alpha(n-1) - \alpha_g) < \pi/2) t(n) = cos(\alpha(n-1) - \alpha_g); elseif = t(n) = 0 \tag{5}$$

$$\alpha(n) = t(n)\alpha(n-1) + (1 - t(n)\alpha_g) \tag{6}$$

Figure 4 illustrates one of the multiple tests used to verify the model efficiency. An experimented welder has filled in the notebook for a thick multiple-pass weld with 31 passes. In this case, the welding position is horizontal–vertical. Two different chemical etchings reveal grain orientation (Figure 4a) and passes (Figure 4b). Simulated grain orientation is showed in Figure 4c. For image analysis, grain orientations are represented in square meshes of 2 × 2 mm^2. MINA parameters are R_L= 0.39, R_V = 0.25, θ_B = 36°, θ_C = 28° and n = 10. Angle parameters θ_B and θ_C are more important than those of flat welds. Part (d) in Figure 4 represents differences between measured orientations on micrographs using level lines; the darker areas correspond to higher differences. The MINA model gives orientation maps with an average error of 10 to 15° for classical flat welding, with a standard deviation of 10° [60,61].

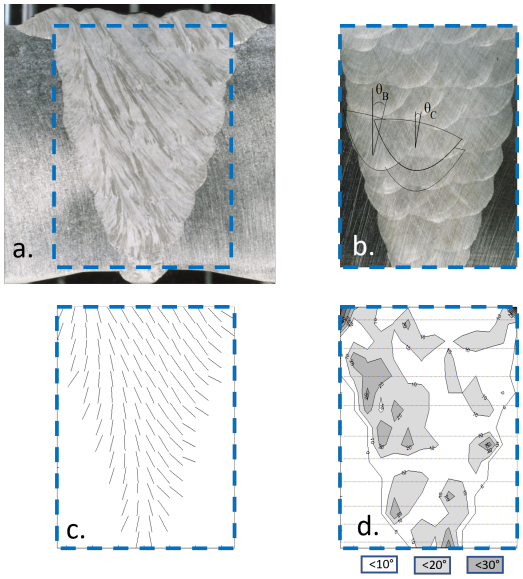

Figure 4. Example of modelling results for horizontal–vertical welding.

In the case of horizontal–vertical welding, the grain map is greatly non-symmetrical, because of the remelting of passes and the manual incline of the electrode. This modelling performed with the MINA model has been a great advance in the field, as this information was absolutely not predicted before, and the purely geometrical models only provided

simplified descriptions of the weld. Furthermore, studies have demonstrated that if the average error reaches 20° or more, this indicates that there is a strong error in the welding notebook: several passes are missing, for instance, or the order of passes were not correctly reported.

The MINA model has also been used in the case of a bimetallic stainless steel weld [62]. In this study, there is a difficulty, as the metallography analysis shows that the order of passes may be read in two different ways. Nevertheless, the grain orientation is correctly predicted, with a better accuracy than with an analytical model. The study confirms that the knowledge of the correct order of passes is very important for the calculation of the grain map. Nowers et al. use the MINA model to supply representative anisotropic weld maps in a complete UT simulation for parametric studies of defect detection [63]. They use a semi-analytical model to simulate the degradation of ultrasonic images caused by the propagation through an anisotropic austenitic material. Ray-tracing calculation is performed with the A* path-finding algorithm.

4. Extension of the MINA Model to Gas Tungsten Arc Welding

Gas tungsten arc welding (GTAW) is often operated in addition to shielded metal arc welding (SMAW) for industrial applications. Some experimental investigation with ultrasounds has been conducted on plates welded using these two welding processes to compare their inspectability [64]. In this study, the ultrasonic time-of-flight diffraction (TOFD) technique is investigated to compare the resulting images, as each process creates a specific grain structure and, as a consequence, creates a material with a different anisotropic behaviour. It is shown that the GTAW sample is more isotropic than the SMAW sample. It is demonstrated that the GTAW material exhibits a stronger wave attenuation. It is easier to detect flaws with Bscans for the SMAW sample. It is also noticed that the time of flight of diffraction (TOFD) technique works with better efficiency for SMAW welds than for GTAW welds.

Recently, Marsac et al. proposed an extension of the MINA model [65]. As there are significant differences in the welding parameters between the SMAW process and the GTAW process, the authors choose to apply the MINA main guidelines. If some phenomenological input parameters are obtained from welding notebook data, a new approach is used to define some phenomenological parameters. This approach uses analysis and measurement of the dimensions of simple beads on plate. These kinds of beads are generally available because they have been made for each weld before complete welding in order to adapt welding settings. The welds have been manufactured in a downhand position using GTAW with arc voltage control (AVC). The Figure 5 shows that the pass morphology is different from that obtained with the SMAW process, as seen in Figure 5a. In Figure 5b, a sketch of a weld bead is drawn, with four measured geometrical parameters: the bead width W_b, the bead height H_b, the reinforcement R_b and the bead penetration depth D_b. Figure 5c represents the simplified geometric model for a pass in the GTAW weld: a "U-flat" type. Marsac has tested various welding parameters, and obtained in any case this type of pass morphology. Remelting parameter R_v is the ratio of D_b to H_b; this ratio depends on the welding power. For small powers, the average of R_v values is 0.39, and for high powers, it is 0.61. The R_L parameter cannot be evaluated simply from the measurements of the widths and the heights on the beads. The study shows that R_L values are also related to several other parameters such as the layer width, the number of passes per layer and the width of each pass [65]. R_L keeps an identical value within the same layer, but can be modified from one layer to another.

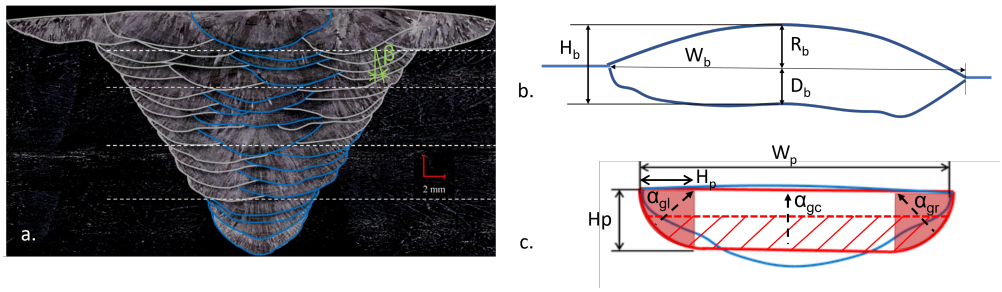

Figure 5. Analysis of GTAW pass morphology. (**a**) passes shape. (**b**) bead parameters. (**c**) simplified geometry for modelling.

Following previous MINA model guidelines, grain growth is closely connected to the temperature gradient. The new model considers three areas, as shown in Figure 5b. Black arrows represent grain growth directions, which are considered symmetric about the vertical axis. The central area is defined as a rectangle and the lateral zones are defined with a quarter circle. These lateral zones contain continuously varying grain growth orientations. In the central zone the grain growth direction is mainly vertical. Figure 5c shows with black arrows that the grain growth at boundaries is assumed to be orthogonal to boundaries. This principle follows MINA basic rules, that is, it considers that boundaries correspond to an isotherm and the temperature gradient is perpendicular to these lines. Grains within a bead are straight; it is thus assumed that the temperature gradient is also straight. The grains do not cross each other within a pass, and so selective growth is rarely observed. Using these hypotheses and considering the "U-flat" geometry, it is possible to automatically calculate the thermal gradient directions α_g. As for the SMAW process, the extension of the MINA model takes into account the incline of the pass deposit, this incline varying according to the spatial position related to the chamfer. When a pass is at the boundary of the chamfer or when a pass rests laterally on a single pass, the grain orientation is greatly inclined, corresponding to a global inclination of the thermal gradient direction. An example of this phenomenon is shown in Figure 5a, with an incline β. In the case of the last pass in a layer, this pass lies between the two passes that surround it, and the grain orientation is vertical. As a consequence, the directions of the temperature gradient are modified by a value β for all passes except for the last one for each layer. With Equation (7), Marsac proposes to calculate β as the result of the non-symmetrical balance of heat flows [65].

$$\tan\beta = \frac{H_p(1-R_V)(1+\frac{H_p}{H_p+W_p})}{W_p + H_p(1-R_V)(\frac{W_p}{H_p+W_p})} \tag{7}$$

The orientation of a grain in a mesh (i,j) depends on other orientation directions in adjacent meshes and depends on the local temperature gradient. An epitaxy rule is defined using the difference between the average direction in the mesh (i,j) neighbourhood and the gradient direction at this location. If this difference is greater than 40°, the grain direction follows the gradient direction. For meshes close to the chamfer, the grain directions are defined equal to the temperature gradient direction.

The extension of the MINA model proves to be consistent. This has classically been assessed using the comparison between grain growth directions obtained with metallographic analysis and with directions calculated by the model. Two map examples from [65] are reported in Figure 6.

The evaluation of grain directions is made with a mesh size of $0.5 \times 0.5\ mm^2$. A global average error θ_G and the standard deviation σ_G are calculated. This global error is correlated to the grain orientation differences within the weld, but also along the chamfer and free surface. In the latter case, differences can be higher due to the geometric limitations of the model: the pass shape is defined as a rectangle, a straight chamfer that does not take into account the dilution at chamfer boundaries and simplification in the modelling of the

incline of passes. A second average error θ_W is then calculated within the welded area. The corresponding standard deviation is, in that case, σ_W.

For Figure 6a, the global statistics are $\theta_G = 20^\circ$ and $\sigma_G = 16.4^\circ$, and become $\theta_G = 18.2^\circ$ and $\sigma_G = 15.5^\circ$ in the welded zone. For Figure 6b, the global statistics are $\theta_G = 13.8^\circ$ and $\sigma_G = 15.2^\circ$, and in the welded zone, $\theta_G = 11.8^\circ$ and $\sigma_G = 12.7^\circ$. Modelling differences within the welded areas are small, a little higher than average results obtained for SMAW welds. Results demonstrate that the extension of the MINA model is in good agreement with the metallography analysis for GTAW welds.

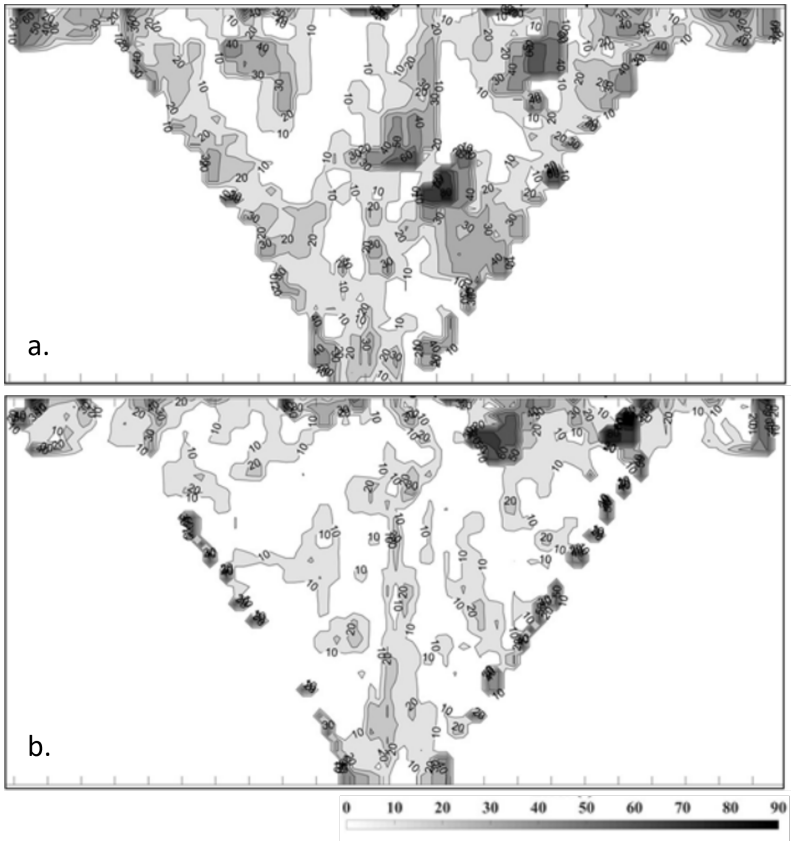

Figure 6. Two examples (**a**,**b**) of grain orientation difference in ° for GTAW.

5. Inverse Approaches for Improving or Defining Grain Orientation Maps

In previous sections, ultrasonic measurements were not used to improve grain description. As mentioned in our introduction, the issue of defining grain orientation is permanently related to advances in numerical codes used to simulate ultrasonic wave propagation. For a complete UT simulation, the direct model firstly includes material description, as it is discussed here, and then a wave propagation code to simulate the ultrasonic testing. Such simulation helps NDT experts to analyse defect detection possibilities. The inverse approach aims to use UT measurements to describe grain orientation. Several authors have used an initial grain orientation map and then proposed algorithms using UT measurements to modify the initial map to improve correlation between UT prediction and UT measurement. In an inverse approach, simulated results are compared with experimental ones, and a cost function measures the similarity between simulation and experimental results. An optimisation algorithm is then used to modify model parameters to improve this similarity until it is low enough for the inverse approach to be stopped.

This inverse approach was tested with the MINA model coupled with the ATHENA code [66–68]. In [68], the attenuation of the waves is not taken into account, and so the amplitude values calculated with the simulation cannot be easily compared with those reported on the experimental curves. It is not possible to construct an inverse approach with

experimental measures. Fictitious experimental data are produced with the ATHENA code. This approach is defined as inverse crime, but it is useful to demonstrate the capability of an inverse approach. In the work performed by Gueudré et al., the goal is to improve the values of the four main parameters: the two remelting parameters (the lateral remelting rate R_L and the vertical remelting rate R_V) and the two angle parameters (θ_B and θ_C). A previous sensitivity analysis confirmed their importance for the MINA model. The algorithm compares the complete echodynamic curve obtained on the other side of the weld using a through transmission technique for several transducer positions (i = 1 to NbTrPo) and the simulated curve obtained using the ATHENA code. The echodynamic curve is calculated for several positions (j = 1 to NbPo). The cost function measures the quadratic distance between the simulated echodynamic curve ($e_j^{i,sim}$) and the real curve ($e_j^{i,exp}$):

$$J(R_L, R_V, \theta_B, \theta_C) = \sum_{n=1}^{NbPo} \sum_{n=1}^{NbMePo} \left(\frac{e_j^{i,sim}(R_L, R_V, \theta_B, \theta_C) - e_j^{i,exp}}{e_j^{i,exp}} \right)^2 \quad (8)$$

The optimisation function uses genetic algorithms to ensure a global optimisation. Four parameters are evaluated together. The algorithm stops when the cost functions calculated with nine generations remain unchanged. The inverse solution is found before 20 generations. This study demonstrates that inversion of the modelling problem is possible using the four main MINA variables. It is pointed out that the most important point is to know the order of passes. Whenever the welding notebook is unreliable or missing, the order of passes should be reconstructed. A first attempt has been made to solve such inverse problem order of passes [69], but it is a very complex mathematical issue.

This strategy is applied by Fan et al. in [70]. The novelty is to propose a measurement setting where there is no need to access the remote side of a butt-welded plate. An ultrasonic array is used on a single side to construct a useful weld map of the spatial variations in anisotropic stiffness orientation. In their approach, they replace echodynamic curves by measurements of the arrival time at chosen locations to reduce uncertainties of attenuation in the welded material and uncertainties due to coupling.

This inverse approach using a genetic algorithm to improve the initial weld grain map was also used by Liu et al. in [71] with a multiobjective algorithm. The weld map is divided in 34 subregions; the weld is vertically symmetrical, so only 17 values have to be optimised. The experimental setup uses two angles: 45° and 60°; and two types of waves: a P wave and a S wave. The positions of the peaks in a pitch–catch configuration are used to compare simulation and experiments.

The success of the inverse approach depends on a very good knowledge of the parameters and the uncertainty on the values of the elasticity constants C_{ijkl}. These values are major input parameters for the simulation, as pointed out by Gueudré et al. [72]. These values are difficult to evaluate experimentally. Phased array transducers bring new solutions to make measurements with various angles without moving the measuring receiver. To improve their results, they use a seismogram, which corresponds to the signals recorded on each element in the line array. In this study, it is shown that the influence of the C_{ijkl} is highly dependent on the measurement setup (position of the sensors relative to the weld). The authors recommend characterising the weld material with in situ measurements before making the ultrasonic test itself.

6. Concluding Remarks and Further Research

We have described and explained a continuous research effort made over more than twenty years to model a welded material microstructure for ultrasonic testing simulation. All the steps proposed in the introductory figure (Figure 1) have now been investigated in detail, and complete solutions are available for industrial applications. Research advances are here discussed to continue to improve the quality of simulation predictions or to enlarge the field of applications for existing solutions. Three axes for further research can

be identified. The first axis is aiming at improving the prediction of the wave attenuation. The second axis for further research is the optimisation of the grain map. The third axis is obtaining the real weld geometry instead of a simplified geometry.

The question of wave attenuation is not discussed in details. Wave attenuation is very difficult to take into account both for the modelling part and for the experimental part. The intrinsic attenuation of a material is a mechanism very difficult to quantify. In many situations, the diagnosis to validate material knowledge is based on velocity measurements and thus based on time of flight values. It requires precise wave path prediction, which is why very good material description is mandatory. The use of wave amplitude is more difficult, both experimentally and in simulation, as attenuation also has an anisotropic behaviour and data are scarce in the literature on the subject, mainly because precise measurements require strong efforts to eliminate all transducer effects (definition, position, etc.). In combination with the study of C_{ijkl}, we have taken into account this question in many previous papers, and more specifically, we have used attenuation measurements made during several specific studies [73]. Ploix and al. [74] developed dedicated experimental studies based on the decomposition of the beam into a plane wave angular spectrum and on the calculation of transmission coefficients in the k-space domain. Solving Christoffel's equation at the corresponding boundary conditions makes it possible to calculate transmission coefficients. The material symmetry should be chosen in the monoclinic case. It is difficult to align the material internal symmetry axis with the symmetry axis of the ultrasonic measurement setup. If there is a difference between these two axes, the material exhibits a monoclinic behaviour. The experimental results obtained are in accordance with theoretical behaviours predicted by Hirsekorn's theory [75] and Ahmed's work [76]. These values are considered now as reference values in several codes for austenitic weld materials (ATHENA or CIVA codes). Attenuation properties (or the imaginary part of C_{ijkl}) should be properly taken into account in any inverse problem that uses amplitude measurements to investigate welds using ultrasonic images. In the MUSCAD project, it is mentioned that there is a bigger uncertainty of the imaginary part of the C_{ijkl}, which is very difficult to evaluate. It may produce significant differences between simulated and real attenuation [72]. Attenuation is also closely related to the shape and the distribution of the grains. Studies about microstructure noise also play a part in the necessary understanding of the attenuation mechanisms. Such studies are not discussed here; important work on the subject is presented in Ahmed's work [76]. Finite element modelling has been used to evaluate the effect of various grain distributions on the ultrasonic noise. Three dimensional simulations are now possible [77]. It still requires heavy computational workflow; hopefully this drawback can be reduced in years to come.

To reduce the attenuation impact and to limit the beam-splitting phenomenon in dissimilar welded material, Hwang et al. [78], propose to apply phased arrays to enlarge the ultrasonic energy, thereby improving the potential to detect cracks.

Welded material is not always described at a very thin scale (a millimetre one) but over larger areas [79] using macrographic examination on representative welds to propose welded material definition. The material description is based on an averaged grain orientation. Further development for MINA modelling could consist of proposing an automatic definition of this kind of zone of interest by automatically clustering material meshes in larger areas. Advances in various artificial intelligence algorithms clearly make this research way possible, even if it would require more available macrograph data to cover as many welding cases as possible. The best situation to develop a weld-related algorithm would be to have the initial welding notebook. That is a real difficulty in many cases, specifically when nondestructive inspection should be applied to help to assess the structural integrity of aged welded structures. However, a major drawback is the risk of obtaining not-so-accurate ultrasound paths. When few hypotheses are possible in weld manufacturing, it is still possible to reconstruct welded material without using solidification laws in detail. Algorithms are developed by considering the material locally, and of course by trying to obtain the local grain orientation. A number of studies can be

found in the literature that take the benefit of multiple array measurements. As indicated, reconstruction is performed using time of flight data. Tant et al. [80] proposed a forward model to simulate the wave front propagation in an anisotropic medium. It is combined with the reversible-jump Markov chain Monte Carlo approach to modify grain orientations. Significant improvement across multiple metrics developed to characterise flaws is shown. Methods like the total focusing method (TFM) have the potential to reconstruct welded material thanks to image optimisation. More recently, Ménard et al. [81] developed an algorithm for homogeneous austenitic material. Ultrasonic image enhancement is searched for in unknown anisotropic steels. An optimisation algorithm modifies the unknown variables to optimise the quality of TFM images. Experiments are performed on two industrial components. The potential of neural networks is also investigated to help describe welded material. A framework is proposed that uses deep neural networks (DNNs) in combination with a dedicated experimental setup with full aperture, pitch–catch and pulse–echo transducer configurations to reconstruct material maps of grain orientation [82]. The objective is to obtain real-time imaging to unlock a large range of applications for ultrasonic testing, making in-process inspection during manufacturing possible.

Among the possible improvements to make to all these methods developed to define welded material considering the weld geometry definition, indeed, a first typical input is the geometry of the weld, often a V-shaped weld. But it is known that during the welding processes, residual stresses and distortions occur. Numerical process simulation provides the evolution of physical quantities such as temperature, strains and stresses at each point in the welded component. Three-dimensional simulations are needed to accurately predict weld distortions in the case of multipass welding. In their work, Duranton et al. [83] made a three-dimensional finite element simulation of the multipass welding of a stainless steel pipe with thirteen passes. Computed distortions and residual stresses are calculated. Experimental measurements show that the chamfer presents a distortion of several millimetres after five passes. It is observed regularly that the largest differences between modelled orientations and those measured on the macrograph are near the weld chamfers. This is the result of a MINA model simplification, as a parabolic shape of the pass is used, and there is no specific refined part to fill the potential remaining volume between the passes and the initial chamfer geometry. This difference is clearly seen when an inverse method is tested to evaluate the remelting of passes. A possible way of progress is to use ultrasonic measurements to define the real weld shape. The process could be similar to some methods developed in medical imaging to extract a volume from ultrasonic data. In their work, Provencal and Laperrière [84] use a deep learning framework to automatically identify and localise the geometry of welds. A three-dimensional representation of the weld structure can be directly obtained from the ultrasound measurement.

As underlined by Sun et al. [85] in a recent study, as computer power increases and the number of qualified inspectors declines, there is a growing interest in automation including the analysis of data. Machine learning has the potential to provide a solution to enhance nondestructive examination reliability. Nevertheless, specific literature appears to produce limited information on several issues, including data set and sample size determination. There is often limited information included, making it difficult to reproduce results or to evaluate uncertainty or probability of detection.

All these developments in microstructure modelling for ultrasonic testing from SMAW to GTAW are giving robust knowledge that could be included in precise simulations for ultrasonic nondestructive testing and could be used industrially with many objectives. Computer performance also makes it possible to develop inverse approaches to obtain grain orientation maps when no metallographic observations are available. But as the ultrasonic inspection is closely dependent on the weld structure, the more physical laws are included, the more the prediction will be very efficient. Most of studies considered a 2D material description. It is known that there are 3D effects in the case of welding in position, such as the overhead position, preliminary studies [73] show a slight incline of the grain

structure. There is a need for more complete studies to be able to propose a 3D modelling from the MINA model.

All these developments in material modelling have been made concurrently with the development of inverse approaches, welding modelling and artificial intelligence algorithms, and ideally, it would be necessary to use the benefits of all of these advances to go further in the nondestructive inspection of welds. One challenge is to bring this global and multidisciplinary knowledge to the end users, i.e., the NDT inspectors and to help them, by sharing this knowledge, to improve inspection efficiency. Such knowledge sharing will participate in reducing human errors by a better understanding of the challenges faced during weld inspection. Of course, all these studies demonstrate that great advances are possible in weld inspection if more attention is paid to the design for inspectability. This last subject requires continuous cooperation between materials, welding and NDT scientists.

Author Contributions: Conceptualisation, J.M.; methodology, J.M.; software, J.M., C.G., M.-A.P. and G.C.; validation, J.M., C.G., M.-A.P. and G.C.; formal analysis, J.M.; investigation, J.M., C.G., M.-A.P. and G.C.; resources, J.M., C.G., M.-A.P. and G.C.; data curation, J.M.; writing—original draft preparation, J.M.; writing—review and editing, J.M., C.G., M.-A.P. and G.C.; visualisation, J.M.; supervision, J.M.; project administration, J.M.; funding acquisition, J.M., C.G., M.-A.P. and G.C. All authors have read and agreed to the published version of the manuscript.

Funding: This study received no external funding.

Institutional Review Board Statement: Not applicable.

Informed Consent Statement: Not applicable.

Conflicts of Interest: The authors declare no conflicts of interest.

References

1. Heinrich, T. *Warship Builders: An Industrial History of U.S. Naval Shipbuilding, 1922–1945*; Studies in Naval History and Sea Power; Naval Institute Press: Heidelberg, Germany, 2020; 352p.
2. Ditchburn, R.J.; Burkle, S.K.; Scala, C.M. NDT of welds: State of the art. *NDT&E Int.* **1996**, *29*, 111–117.
3. Corneloup, G.; Gueudré, C.; Ploix, M.A. *Non-Destructive Testing and Testability of Materials and Structure*; EPFL Press English Imprint: Lausanne, Switzerland, 2021.
4. Birac, C.; Samman, J. A French qualification commission for certifying the performance of Non-Destructive Testing. In Proceedings of the 3rd International Conference on NDE in Relation to Structural Integrity for Nuclear and Pressurized Components, Sevilla, Spain, 14–16 November 2001.
5. Champigny, F. Inspection program for primary system: A new approach. In Proceedings of the 3rd International Conference on NDE in Relation to Structural Integrity for Nuclear and Pressurized Components, Sevilla, Spain, 14–16 November 2001.
6. Rouhan, R.A.; Schoes, F.; Labeyrie, J. Probabilistic analysis of non-destructive testing of offshore structures for evaluating their mechanical integrity. *RFM* **2000**, 235–241.
7. Thompson, R.B. Quantitative Ultrasonic Nondestructive Evaluation Methods. *J. Appl. Mech.* **1983**, 1191–2001. [CrossRef]
8. Thompson, R.B.; Thompson, D.O. Ultrasonics in Nondestructive Evaluation. *Proc. IEEE* **1985**, 1716–1755. [CrossRef]
9. Achenbach, J.D. Quantitative non-destructive evaluation. *Int. J. Solids Struct.* **2000**, *37*, 13–27. [CrossRef]
10. Achenbach, J.D. Modeling for quantitative non-destructive evaluation. *Ultrasonics* **2002**, *40*, 1–10. [CrossRef] [PubMed]
11. Dillstrom, P. Pro-SINTAP—A probabilistic program implementing the SINTAP assessment procedure. *Eng. Fract. Mech.* **2000**, *67*, 647–668. [CrossRef]
12. Schmitz, V.; Kroning, M.; Rooos, E.; Blind, D.; Eisele, U. Planning and use of condition-dependent NDT for the interaction between fracture mechanics and quantitative NDT. *Nucl. Eng. Des.* **2001**, *206*, 291–309. [CrossRef]
13. Ainsworth, R.A. Foreword Special Issue on flaw assessment method. *Int. J. Press. Vessel. Pip.* **2000**, *77*, 853. [CrossRef]
14. Faidy, C.A. RSE-M. A general presentation of the French codified flaw evaluation procedure. *Int. J. Press. Vessel. Pip.* **2000**, *77*, 919–927. [CrossRef]
15. Silk, M.G.; Stoneham, A.M.; Temple, J.A.G. *The Reliability of Non-Destructive Inspection. Assessing the Assessment of Structures under Stress*; Adam Hilger: Bristol, UK, 1987.
16. Nichols, R. The role of non-destructive. *Nucl. Eng. Int.* **1983**, *28*, 29–30.
17. Nichols, R. The use of fracture mechanics and non-destructive testing to reduce the risk of catastrophic failure. *Nucl. Eng. Des.* **1983**, *87*, 3–33. [CrossRef]
18. Wu, W.F.; Syau, J.J. A study of risk-based non destructive in-service inspection. *Nucl. Eng. Des.* **1995**, *158*, 409–415.
19. Sukhorukov, V.V.; Slesarev, D.A.; Shpakov, I.I.; Volokhovsky, V.Y.; Vorotonsov, A.N.; Shalashilin, A.D. Nondestructive Inspection Quantification and Aviation Safety. *Mater. Eval.* **2002**, *60*, 845–847.

20. Larouzee, J.; Martin, E.; Calmon, P. Human Reliability Assessment method applied to investigate human factors in NDT—The case of the interpretation of radiograms in the French nuclear sector. In Proceedings of the NDE in Nuclear Conference, Shefield, UK, 27–29 June 2023. . [CrossRef]
21. Wald, D.J. Slip history of the 1995 Kobe, Japan, earthquake determined from strong motion, teleseismic, and geodetic data. *J. Phys. Earth* **1996**, *44*, 489–503. [CrossRef]
22. Bode, M.D.; Holle, M.J. *Literature Review of Weak Adhesive Bond Fabrication and Nondestructive Inspection or Strength Measurement*; Technical Report DOT/FAA/TC-14/39; FAA: Atlantic City, NJ, USA, 2015; 93p.
23. Galy, J.; Moysan, J.; El Mahi, A.; Ylla, N.; Massacret, N. Controlled reduced-strength epoxy-aluminium joints validated by ultrasonic and mechanical measurements. *Int. J. Adhes. Adhes.* **2017**, *72*, 139–146. [CrossRef]
24. Nichols, R.W. A review of the work related to defining the reliability of non-destructive testing. *Nucl. Eng. Des.* **1989**, *114*, 1–32. [CrossRef]
25. Lemaitre, P.; Koblé, T.D.; Doctor, S.R. Summary of the PISC round robin results on wrought and cast austenitic steel weldments, part III: Cast-to-cast capability study. *Int. J. Press. Vessel. Pip.* **1996**, *69*, 33–44. [CrossRef]
26. Lemaitre, P.; Koblé, T.D.; Doctor, S.R. Summary of the PISC round robin results on wrought and cast austenitic steel weldments, part II: Wrought-to-cast capability study. *Int. J. Press. Vessel. Pip.* **1996**, *69*, 21–32. [CrossRef]
27. Reale, S.; Tognarelli, L.; Crutzen, S. The use of fracture mechanics methodologies for NDT results evaluation and comparison. *Nucl. Eng. Des.* **1995**, *158*, 397–407. [CrossRef]
28. Reale, S.; Tognarelli, L.; Crutzen, S. Structural integrity signifance of round robin testing trials. Application to PISC III Action 3. *Nucl. Eng. Des.* **1995**, *157*, 257–268. [CrossRef]
29. Imperiale, A.; Leymarie, N.; Fortuna, T.; Demaldent, E. Coupling Strategies Between Asymptotic and Numerical Models with Application to Ultrasonic Non-Destructive Testing of Surface Flaws. *J. Theor. Comput. Acoust.* **2019**, *27*, 1850052. [CrossRef]
30. Calmon, P. Trends and Stakes of NDT Simulation. *J. Nondestruct. Eval.* **2012**, *31*, 339–341. [CrossRef]
31. Royer, E.D. *Elastic Waves in Solids I, Free and Guided*; Springer: Berlin/Heidelberg, Germany, 2000; 374p.
32. Ducret, D.; El Guerjouma, R.; Guy, P.; Rńili, M.; Baboux, J. Characterisation of anisotropic elastic constants of continuous alumina fibre reinforced aluminium matrix composite processed by medium pressure infiltration. *Compos. Part A* **2000**, *31*, 45–55. [CrossRef]
33. Chassignole, B.; Villard, D.; Dubuget, M.; Baboux, J.C.; Guerjouma, E. Characterization of austenitic stainless steel welds for ultrasonic NDT. *AIP Conf. Proc.* **2000**, *509*, 1325–1332.
34. Ogilvy, J. Computerized ultrasonic ray tracing in austenitic steel. *NDT&E Int.* **1985**, *18*, 67–77.
35. Silk, M. A computer model for ultrasonic propagation in complex orthotropic structures. *Ultrasonics* **1981**, *19*, 208–212. [CrossRef]
36. Spies, M.; Kroning, M. Ultrasonic inspection of inhomogeneous welds simulated by a gaussian beam superposition. In *Review of Progress in Quantitative Nondestructive Evaluation*; AIP Publishing: Melville, NY, USA, 1999; Volume 18A, pp. 1107–1113.
37. Schmitz, V.; Walte, F.; Chakhlov, S. 3D ray tracing in austenite materials. *NDT&E Int.* **1999**, *32*, 201–213.
38. Langerberg, K.; Hannemann, R.; Kaczorowski, T.; Marklein, R.; Khoeler, B.; Schurig, C.; Walte, F. Application of modeling techniques for ultrasonic austenitic weld inspection. *NDT&E Int.* **2000**, *33*, 465–480.
39. Halkjaer, S.; Sorensen, M.; Kristensen, W. The propagation of ultrasound in a austenitic weld. *Ultrasonics* **2000**, *38*, 256–261. [CrossRef]
40. Gengembre, N.; Lhémery, A. Pencil method in elastodynamics: Application to ultrasonic field computation. *Ultrasonics* **2000**, *38*, 495–499. [CrossRef] [PubMed]
41. Lhémery, A.; Calmon, P.; Lecoeur-Taibi, I.; Raillon, R.; Paradis, L. Modelling tools for ultrasonic inspection of welds. *NDT&E Int.* **2000**, *33*, 495–499.
42. Apfel, A.; Moysan, J.; Corneloup, G.; Chassignole, B. Simulations of the influence of the grains orientations on ultrasounds. In Proceedings of the 16th World Conference on NDT, Montreal, QC, Canada, 30 August–3 September 2004.
43. Liu, Q.; Wirdelius, H. A 2D model of ultrasonic wave propagation in an anisotropic weld. *NDT&E Int.* **2007**, *40*, 229–238.
44. Kolkoori, S.; Rahman, M.U.; Chinta, P.K.; Ktreutzbruck, M.; Rethmeier, M.; Prager, J. Ultrasonic field profile evaluation in acoustically inhomogeneous anisotropic materials using 2D ray tracing model: Numerical and experimental comparison. *Ultrasonics* **2013**, *53*, 396–411. [CrossRef]
45. Kim, Y.; Cho, S.; Park, I. Analysis of Flaw Detection Sensitivity of Phased Array Ultrasonics in Austenitic Steel Welds According to Inspection Conditions. *Sensors* **2021**, *21*, 242. [CrossRef] [PubMed]
46. Boettinger, W.; Coriel, S.; Greer, A.; Karma, A.; Kurz, W.; Trivedi, R. Solidification microstructures: Recent developments, future directions. *Acta Mater.* **2000**, *48*, 43–70. [CrossRef]
47. David, S.; Vitek, J. Correlation between solidification parameters and weld microstructures. *Int. Mater. Rev.* **1989**, *34*, 213–245. [CrossRef]
48. Matsuda, F.; Nakagawa, H.; Lee, J. Weld cracking in duplex stainless steel II. Modeling of cellular dendritic growth during weld solidification. *Trans. JWRI* **1989**, *34*, 107–117.
49. Kurz, W.; Giovanola, B.; Trivedi, R. Theory of microstructural development during rapid solidification. *Acta Mater.* **1986**, *34*, 823–830. [CrossRef]
50. Rappaz, M.; David, S.; Vitek, J.; Boatner, L. Analysis of Solidification Microstructures in Fe-Ni-Cr Single-Crystal Welds. *Metal. Trans. A.* **1990**, *21A*, 1767–1782. [CrossRef]

51. Rappaz, M.; Gandin, C.; Desbiolles, J.; Thevoz, P. Prediction of Grain Structures in Various Solidification Processes. *Metal. Trans. A* **1996**, *27A*, 695–705. [CrossRef]
52. Gandin, C.; Rappaz, M. A coupled finite element-cellular automaton model for the prediction of dendritic grain structures in solidification processes. *Acta Met. Mater.* **1994**, *42*, 2233–2246. [CrossRef]
53. Dilthey, U.; Pavlik, V.; Reichel, T. Numerical simulation of dendritic solidification with modified cellular automata. In *Proceedings of the Third International Meeting on the Numerical Analysis of Weldability*; Number 3 in Mathematical Modelling of Weld Phenomena; Cerjak, H., Ed.; Institute of Materials: London, UK, 1997; pp. 85–105.
54. Choi, J.; Mazumber, J. Numerical and experimental analysis for solidification and residual stress in the GMAW process for AISI 304 stainless steel. *J. Mater. Sci.* **2002**, *37*, 2143—2158. [CrossRef]
55. Brooks, J.; Baskes, M.; Greulich, F. Solidification modeling and solid-state transformations in high energy density stainless steels welds. *Metal. Trans. A* **1991**, *22A*, 915–926. [CrossRef]
56. Nelson, T.W.; Lipold, J.; Mills, M.J. Nature and evolution of the fusion boundary in ferritic-austenitic dissimilar weld metals. Part I: Nucleation and Growth. *Weld. J.* **1999**, *78*, 329–337.
57. Reed, R.C.; Badheshioa, H. A simple model for multipass steel welds. *Acta Metall. Mater.* **1994**, *42*, 3663–3678. [CrossRef]
58. Muragan, S.; Kumar, P.; Raj, B.; Bose, M. Temperature distribution during multipass welding of plates. *Int. J. Press. Vessel. Pip.* **1998**, *75*, 891–905. [CrossRef]
59. Suzuki, R.; Trevisan, R.; Trevisan, O. Analytical solutions for heat flow in multiple pass welding. *Sci. Technol. Weld. Join.* **2000**, *5*, 63–70. [CrossRef]
60. Moysan, J.; Apfel, A.; Corneloup, G.; Chassignole, B. Modelling the grain orientation of austenitic stainless steel multipass welds to improve ultrasonic assessment of structural integrity. *Int. J. Press. Vessel. Pip.* **2003**, *80*, 77–85. [CrossRef]
61. Apfel, A.; Moysan, J.; Corneloup, G.; Fouquet, T.; Chassignole, B. Coupling an ultrasonic propagation code with a model of the heterogeneity of multipass welds to simulate ultrasonic testing. *Ultrasonics* **2005**, *43*, 447–456. [CrossRef]
62. Ye, J.; Moysan, J.; Song, S.J.; Kim, H.J.; Chassignole, B.; Gueudre, C.; Dupond, O. Influence of welding passes on grain orientation—The example of a multi-pass V-weld. *Int. J. Press. Vessel. Pip.* **2012**, *93–94*, 17–21. [CrossRef]
63. Nowers, O.; Duxbury, D.J.; Drinkwater, B.W. Ultrasonic array imaging through an anisotropic austenitic steel weld using an efficient ray-tracing algorithm. *NDT&E Int.* **2016**, *79*, 98–108. [CrossRef]
64. Tabatabaeipour, S.M.; Honarvar, F. A comparative evaluation of ultrasonic testing of AISI 316L welds made by shielded metal arc welding and gas tungsten arc welding processes. *J. Mater. Process. Technol.* **2010**, *210*, 1043–1050. [CrossRef]
65. Marsac, Q.; Gueudre, C.; Ploix, M.A.; Forest, L.; Baque, F.; Corneloup, G. Realistic Model to Predict the Macrostructure of GTAW Welds for the Simulation of Ultrasonic Non destructive Testing. *J. Nondestruct. Eval.* **2020**, *39*, 80. [CrossRef]
66. Becache, E.; Joly, P.; Tsogka, C. An analysis of new mixed finite elements for the approximation of wave propagation problems. *SIAM J. Num. Anal.* **2000**, *37*, 1053–1084. [CrossRef]
67. Becache, E.; Joly, P.; Tsogka, C. Application of the fictitious domain method to 2D linear elastodynamic problems. *J. Comput. Acoust.* **2001**, *9*, 1175–1202.
68. Gueudré, C.; Le Marrec, L.; Moysan, J.; Chassignole, B. Direct model optimisation for data inversion. Application to ultrasonic characterisation of heterogeneous welds. *NDT&E Int.* **2009**, *42*, 47–55. [CrossRef]
69. Gueudre, C.; Le Marrec, L.; Checkroun, M.; Moysan, J.; Corneloup, G. Search of the Order of Passes of an Austenitic Weld by Optimization of an Inversion Process of Ultrasound Data. In *Review of Progress in Quantitative Nondestructive Evaluation*; AIP Publishing: Melville, NY, USA, 2011; Volume 30, pp. 639–646.
70. Fan, Z.; Mark, A.; Lowe, M.; Withers, P. Nonintrusive Estimation of Anisotropic Stiffness Maps of Heterogeneous Steel Welds for the Improvement of Ultrasonic Array Inspection. *IEEE Trans. Ultrason. Ferroelectr. Freq. Control.* **2015**, *62*, 1530–1543. [CrossRef]
71. Liu, Q.; Wirdelius, H. Estimation of Grain Orientation in an Anisotropic Weld by Using a Model of Ultrasonic Propagation in an Inverse Scheme. *Model. Simul. Eng.* **2014**, *2014*, e637476. [CrossRef]
72. Gueudré, C.; Mailhé, J.; Ploix, M.A.; Corneloup, G.; Chassignole, B. Influence of the uncertainty of elastic constants on the modelling of ultrasound propagation through multi-pass austenitic welds. Impact on non-destructive testing. *Int. J. Press. Vessel. Pip.* **2019**, *171*, 125–136. [CrossRef]
73. Moysan, J.; Gueudré, C.; Ploix, M.A.; Corneloup, G.; Guy, P.; El Guerjouma, R.; Chassignole, B. Advances in ultrasonic testing of austenitic stainless steel welds. Towards a 3D description of the material including attenuation and optimisation by inversion. In *Ultrasonic Wave Propagation in Non Homogeneous Media*; Leger, A., Deschamps, M., Eds.; Springer: Berlin/Heidelberg, Germany, 2009; pp. 15–24.
74. Ploix, M.A.; Guy, P.; Chassignole, B.; Moysan, J.; Corneloup, G.; El Guerjouma, R. Measurement of ultrasonic scattering attenuation in austenitic stainless steel welds: Realistic input data for NDT numerical modeling. *Ultrasonics* **2014**, *54*, 1729–1736. [CrossRef]
75. Hirsekorn, S. Directional Dependence of Ultrasonic Propagation in Textured Polycrystals. *J. Acoust. Soc. Am.* **1986**, *79*, 1269–1279. [CrossRef]
76. Ahmed, S.; Thompson, R.B. Effect of Preferred Grain Orientation and Grain Elongation on Ultrasonic Wave Propagation in Stainless Steel. In *Review of Progress in Quantitative Nondestructive Evaluation*; AIP Publishing: Melville, NY, USA, 1992; Volume 11, pp. 1999–2006.

77. Norouzian, M.; Islam, S.; Turner, J.A. Influence of microstructural grain-size distribution on ultrasonic scattering. *Ultrasonics* **2020**, *102*, 106032. [CrossRef]
78. Hwang, Y.-I.; Sung, D.; Kim, H.-J.; Song, S.-J.; Kim, K.-B.; Kang, S.-S. Propagation and Attenuation Characteristics of an Ultrasonic Beam in Dissimilar-Metal Welds. *Sensors* **2020**, *20*, 6259. [CrossRef]
79. Chassignole, B.; Villard, D.; Dubuguet, M.; Baboux, J.C.; El Guerjouma, R. Characterization of Austenitic Stainless Steel Welds for Ultrasonic NDT. In *Review of Progress in Quantitative Nondestructive Evaluation*; AIP Publishing: Melville, NY, USA, 2000; Volume 20, pp. 1325–1332.
80. Tant, K.M.M.; Galetti, E.; Mulholland, A.J.; Curtis, A.; Gachagan, A. Effective grain orientation mapping of complex and locally anisotropic media for improved imaging in ultrasonic non-destructive testing. *Inverse Probl. Sci. Eng.* **2020**, *28*, 1694–1718. [CrossRef]
81. Ménard, C.; Robert, S.; Miorelli, R.; Lesselier, D. Optimization algorithms for ultrasonic array imaging in homogeneous anisotropic steel components with unknown properties. *NDT&E Int.* **2020**, *116*, 102327.
82. Singh, J.; Tant, K.; Curtis, A.; Mulholland, A. Real-time super-resolution mapping of locally anisotropic grain orientations for ultrasonic non-destructive evaluation of crystalline material. *Neural Comput. Appl.* **2022**, *34*, 4993–5010. [CrossRef]
83. Duranton, P.; Devaux, J.; Robin, V.; Gilles, P.; Bergheau, J.M. 3D modelling of multipass welding of a 316L stainless steel pipe. *J. Mater. Process. Technol.* **2004**, *153–154*, 457–463. [CrossRef]
84. Provencal, E.; Laperrière, L. Identification of weld geometry from ultrasound scan data using deep learning. *Procedia CIRP* **2021**, *104*, 122–127. [CrossRef]
85. Sun, H.; Ramuhalli, P.; Jacob, R.E. Machine learning for ultrasonic nondestructive examination of welding defects: A systematic review. *Ultrasonics* **2023**, *127*, 106854. [CrossRef]